Electronic Supplementary Material (ESI) for Environmental Science: Nano.

Supplementary Information

Combined effect of Cu^0 and oxygen vacancy in Cu-based zeolite enables highly efficient photo-Fenton-like performance for water purification

Wei Zhang, [a] Lan Wang *[a], Chen Hou [a], Zhiqiang Zhu [a], Eric Lichtfouse *[b], Christos Trapalis [c], and Chuanyi Wang [a]

[a] *School of Environmental Science and Engineering, Shaanxi University of Science and Technology, Xi'an 710021, PR China*

[b] *State Key Laboratory of Multiphase Flow in Power Engineering, Xi'an Jiaotong University, Xi'an 710000, PR China*

[c] *Institute of Nanoscience and Nanotechnology, NCSR "Demokritos", Agia Paraskevi 15341, Greece*

* Corresponding author.

E-mail addresses: wanglan@sust.edu.cn; eric.lichtfouse@icloud.com

1. Texts

Text S1. Materials.

Sodium aluminate ($Al_2O_3 \cdot Na_2O$, 98%), Cetrimonium bromide (CTAB, 99%), Sodium hydroxide (NaOH, 98%), Hexamethyleneimine (HMI, 98%), Tetraethylenepentamine (TEPA, 98%), Sodium thiosulfate ($Na_2S_2O_3$, 99%) and Sodium carbonate (Na_2CO_3, 99.8%) were purchased from Aladdin Co., Ltd.. LUDOX AS-40 colloidal silica (40 wt%), Copper (II) sulfate pentahydrate ($CuSO_4 \cdot 5H_2O$, 99%), benzoquinone (BQ, 99%), L-Histidine (99%), and tert-Butanol (TBA, 99%) were purchased from Merck Co., Ltd.. Phenol (99%), 2,4−Dichlorophenol, 4−chlorophenol (Sigma-Aldrich Co., Ltd.). Hydrogen peroxide, Sulfuric acid (Sinopharm Chemical Reagent Co., Ltd.). Silver nitrate (Tianjin Tiangan Chemical Technology Development Co., Ltd.). All reagents were not purified. Deionized water was prepared by pure water meter and was used throughout the experiment.

Text S2. Characterization.

XRD patterns was recorded from 3° to 80° with nickel-filtered Cu Kα radiation (λ = 1.54 Å Rigaku, Smart Lab 9kW). Operating conditions: voltage is 45 kV, scanning rate is 10°/min. TEM was carried out using FEI Talos F200x Microscope, which operating voltage is 200kv. EDS elemental analysis was conducted using Bruker X-Flash SDD 5010. XPS was performed on Thermo SCIENTIFIC K-Alpha spectrometer (Al Kαlph source). The specific surface areas were measured by a surface area analyzer (ASAP2460, Micromeritics, USA) with the Brunauer-Emmett-Teller (BET) method, and the pore size distribution was calculated using BJH calculations method. DRS spectroscopy measurement was recorded on a spectrophotometer (Agilent-Cary 5000, USA) from 200 nm to 1200 nm. FTIR spectra were recorded on a Bruker Vertex70 (4000−400 cm^{-1}). EIS was measure on CHI 660E (Chenhua Co., Ltd., China). The copper leaching during the reaction was measured by an ICP-AES (Thermo Scientific, ICAP 6300 Duo) instrument.

Text S3. Analytic methods.

The degradation was monitored via high performance liquid chromatograph (Ultimate 3000, Thermo Fisher Scientific) with a DAD-300 detector, C18 Hypersil GOLD column at column chamber temperature of 35 °C. The test conditions are as follows: phenol (60% H_2O, 40% methanol, flow rate:

1 mL/min, UV: 283 nm). 4−CP (30% H_2O, 70% methanol, flow rate: 1 mL/min, UV: 224 nm). 2.4−DCP (70% acetonitrile, 30% H_2O, UV: 286 nm). DCF (35% acetic acid aqueous solution (0.1%), 65% acetonitrile, UV: 274 nm). MB and RhB were detected by ultraviolet spectrophotometer.

In addition, EPR was used to detect the involved reaction ROS, 5,5-Dimethyl-1-pyrroline n-oxide (DMPO) was dispersed in different air-saturated methanol and aqueous dispersions. A 300 W Xe lamp ($\lambda > 400$ nm) was used as a visible-light source. In the absence of H_2O_2, a total of 100 μL of DMPO (176.75 mM) was added into 100 μL of the prepared degradation solution (water for •OH, methyl alcohol for $\bullet O_2^-$, 0.2 g/L catalyst, 10 mM H_2O_2, pH 4). Then, the mixed solution was held for 5 min under light. The solution was sucked out by a quartz capillary tube with an inner diameter of 1 mm, and the spectrum was recorded by placing the capillary tube in the EPR cavity. For comparison, H_2O_2 (10 mM) was added into solution before light irradiation to detect the different signals, and other conditions keep constant. The preparation of 2,2,6,6-tetramethyl-4-oxo-piperidine (4-oxo-TEMP) solution is the same as DMPO. 20 mg sample was placed into the sample tube and then into the ESR cavity to detect oxygen vacancy.

TOC of initial and irradiated samples were measured on Elementar TOC analyzer. For EIS test, the ITO glass coating with catalyst was used as a working electrode, and using Pt sheet and Ag/AgCl served as the counter and the reference electrode, respectively. The electrolyte solution: 0.1 M Na_2SO_4.

Text S4. DFT calculations

Gaussian09, D01 software package was used to DFT calculations[1]. We used the B3LYP functional and 6-31G(d) basis (Grimme dispersion corrections, GD3BJ) to optimize the model of pollutants. Then, the singlet point energy calculations were based on the B3LYP functional and a larger 6-311G(d) basis. The Hirshfeld atomic charges, HOMO/LUMO gap, ESP and Fukui functions were achieved with the help of the Multiwfn program[2, 3].Fukui function has been widely used to predict reactive sites of electrophilic, nucleophilic, and radical attacking[4].

2. Table

Table S1. Specific surface area (S_{BET}), pore size (d) and pore volume (Vt) of the samples.

sample	Structural parameters		
	$S_{BET}(m^2/g)$	d(nm)	$V_t(cm^3/g)$
β-zeolite	63.2	27.99	0.41
Cu^0@CuZ	133.9	14.81	0.48

Table S2 The Cu content of Cu^0@CuZ-P and Cu^0@CuZ.

Catalyst	Cu^0 content (%)	Cu^+ content (%)	Cu^{2+} content (%)
Cu^0@CuZ-p	33	29.8	37.2
Cu^0@CuZ	42	24	34
Cu^0@CuZ-p after illumination	33.7	29.6	36.7
Cu^0@CuZ after illumination	41.1	29.5	29.4

Table S3. Degradation conditions and pollutants removal efficiency over Cu^0@CuZ and other catalysts.

target pollutants	catalysts	reaction conditions	catalytic performance	references
phenol	$FeOOH/Bi_2MoO_6$	pH: 3.0; catalyst: 1.0 g/L; $[H_2O_2]$: 20 mM; C_0: 5 mg/L; T: 25 °C	100% removal in 3 h, k = 1.13876 h^{-1}	[5]
phenol	Fe_3O_4-GO	pH: 5.0; catalyst: 0.25 g/L; $[H_2O_2]$: 10 mM; C_0: 20 mg/L; T: 25 °C	100% removal after 120 min, k = –	[6]
phenol	FeOOH quantum dots coupled to g-C_3N_4	pH: 5.0; catalyst: 4 g/L; $[H_2O_2]$: 20 mM; C_0: 50 mg/L; T: 25 °C	100% removal after 90 min, k = 0.054 min^{-1}	[7]
phenol	Cu-iminodisuccinic acid complex	pH: 7.0; catalyst: 0.02 mM; $[H_2O_2]$: 14.7 mM; C_0: 50 mg/L; T: 25 °C	95% removal after 60 min, k = –	[8]
phenol	AG/Fe_3O_4	pH: 7.0; catalyst: 0.5 mg/L; $[H_2O_2]$: 250 mM; C_0: 40 mg/L; T: 25 °C	100% removal after 120 min, k = 0.02083 min^{-1}	[9]
4-CP	$La_{1-x}Ti_xFeO_3$	pH: 3.0; catalyst: 0.5 g/L; $[H_2O_2]$: 3.7 mM; C_0: 25 mg/L; T: 25 °C	100% removal in 200 min, k = 0.0025 min^{-1}	[10]
MB	MA-Cu-Fe@C	pH: 5; catalyst: 0.5 g/L; $[H_2O_2]$: 32 mM; C_0: 50 mg/L; T: 25 °C	98.8% removal after 80 min, k = 0.054 min^{-1}	[11]
RhB	Zn/Co-ZIFs@MIL-101(Fe)	pH: 5; catalyst: 0.2 g/L; $[H_2O_2]$: 90 mM; C_0: 100 mg/L; T: 25 °C	98% removal after 3 h, k = 1.33 h^{-1}	[12]
TC	CuFeO QDs/CNNSs	pH: 6; catalyst: 0.5 g/L; $[H_2O_2]$: 100 mM; C_0: 50 mg/L; T: 25 °C	100% removal in 25 min, k = –	[13]
phenol/MB		pH: 4.0; catalyst: 0.2 g/L; $[H_2O_2]$: 10.0 mM; C_0: 20 mg/L; T: 25 °C	100% removal in 20 min, k = 0.387 min^{-1}	this work

3. Figures

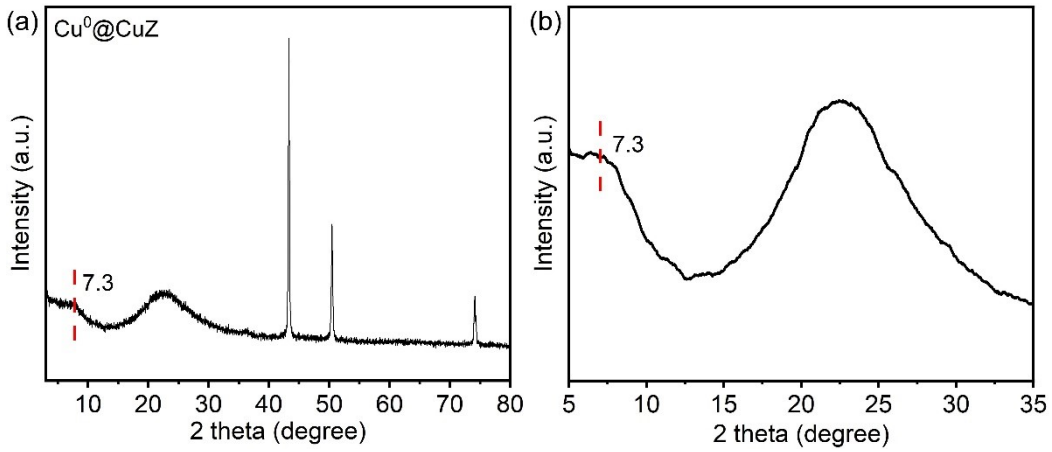

Fig. S1 (a) XRD pattern of Cu^0@CuZ. (b) Enlarged view of the XRD pattern of Cu^0@CuZ.

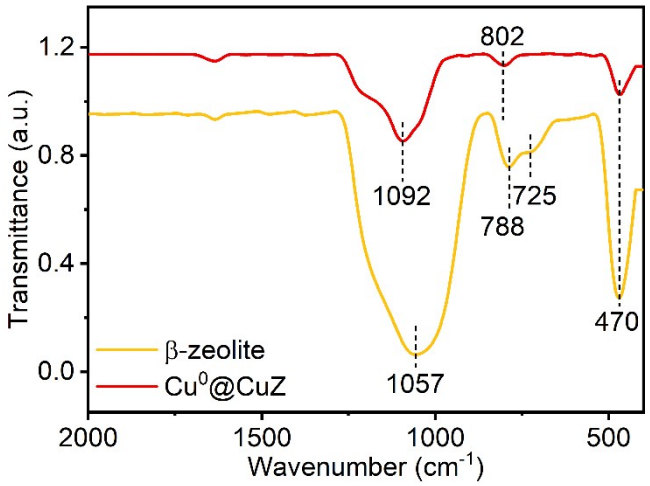

Fig. S2 FTIR spectra of samples.

The FTIR spectrum showed that bands around 470, 725, 788, 1057 cm^{-1} were characterized to β-zeolite. By contrast, an additional band at approximately 1092 cm^{-1} was assigned to Si-O-Cu bond compared with β-zeolite [14-16].

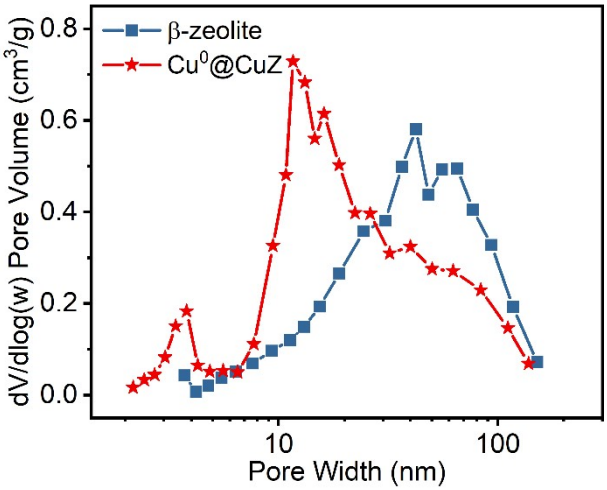

Fig. S3 Pore size distribution of Cu^0@CuZ and β-zeolite.

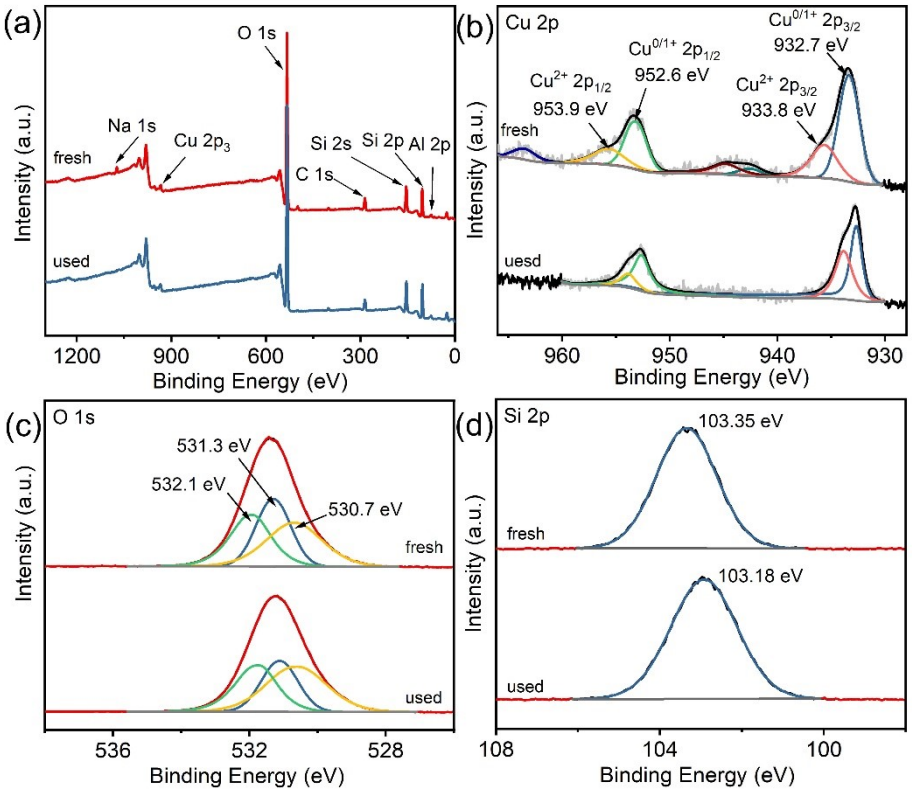

Fig. S4 (a) Wide scan XPS spectrum of Cu^0@CuZ. High-resolution XPS spectra of (b) Cu 2p, (c) O 1s and (d) Si 2p for Cu^0@CuZ.

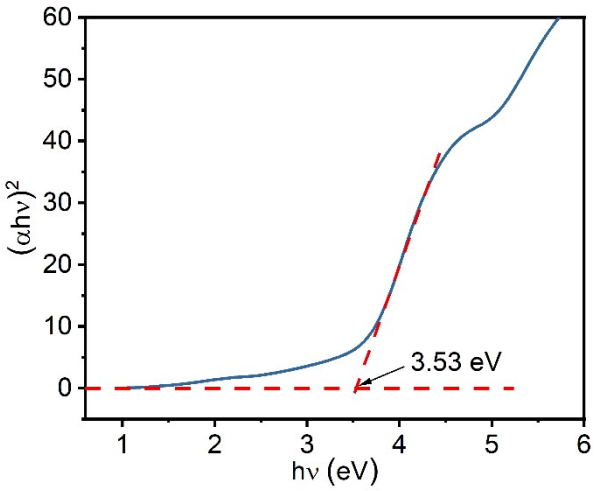

Fig. S5 Band gap values of Cu^0@CuZ-p.

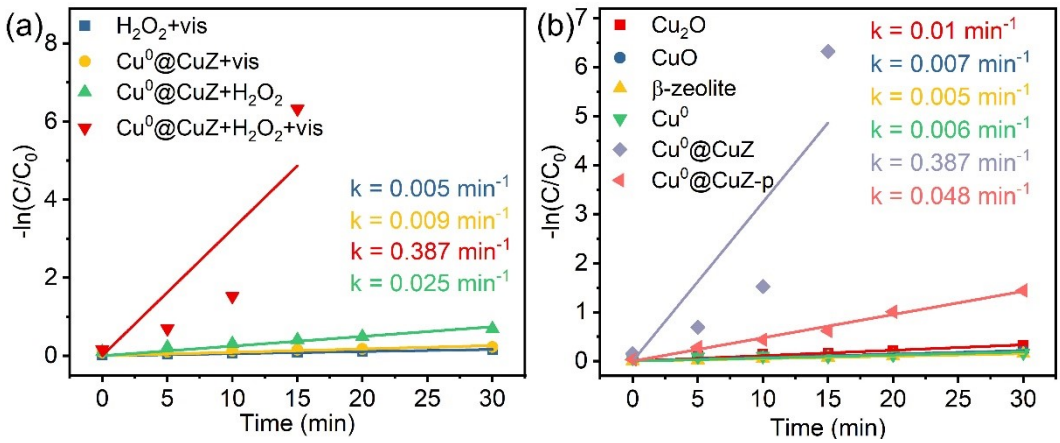

Fig. S6 (a) *k* values of various reaction systems. (b) *k* values over different catalysts in the photo-Fenton-like system.

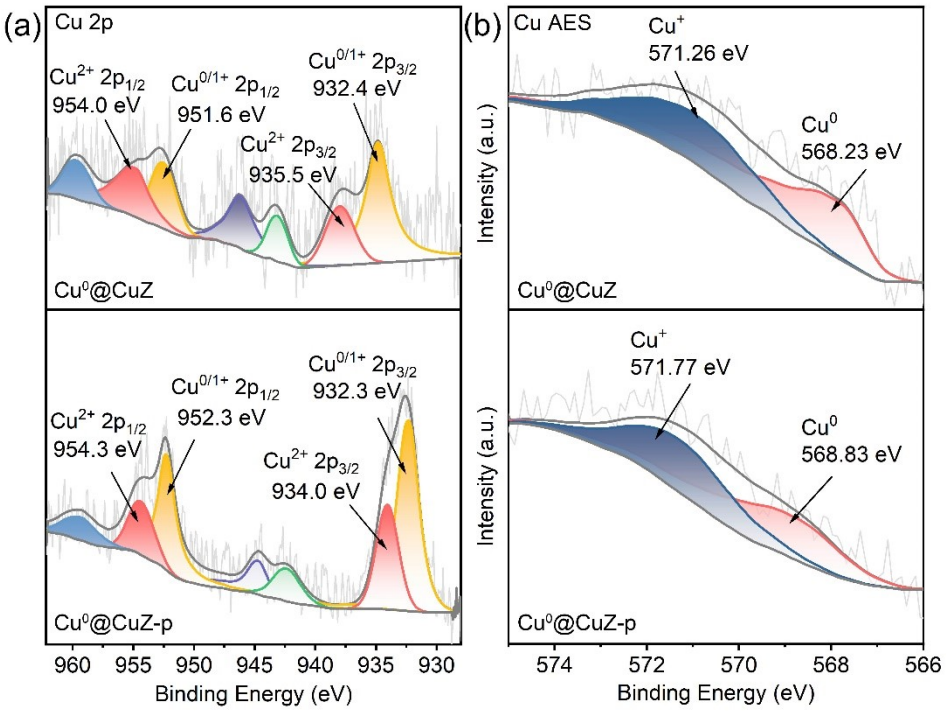

Fig. S7 The high-resolution XPS of Cu 2p and Cu AES spectrum of Cu^0@CuZ and Cu^0@CuZ-p after 30 min illumination.

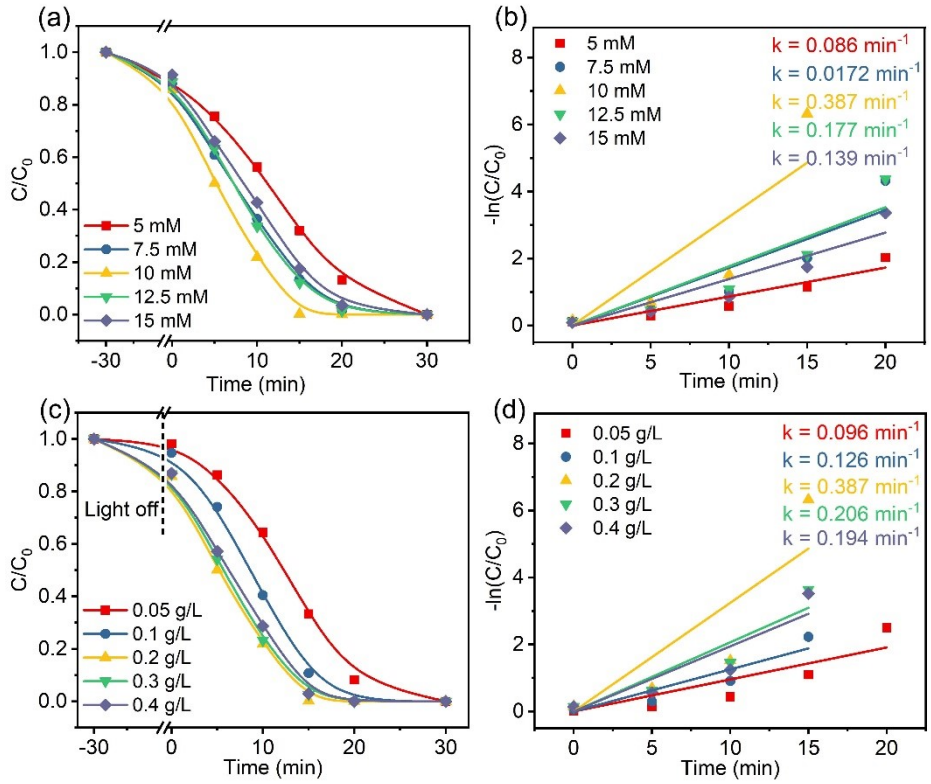

Fig. S8 Effects of (a) H_2O_2 concentration and (b) corresponding *k* value on phenol removal over Cu^0@CuZ. (c) catalyst dosage and (d) corresponding *k* value on phenol removal over Cu^0@CuZ.

As depicted in Figs. S6a-b, the phenol removal efficiency increased from 87% to 100% when H_2O_2 concentration raised from 5 to10 mM, and the k value of Cu^0@CuZ markedly increased from 0.086 to 0.387 min^{-1}, which was due to the increasing concentration of H_2O_2 can produce more •OH for phenol removal. However, both the removal efficiency and the k value decreased as the H_2O_2 concentration further increased to 15 mM, which is due to the fact that the excessive H_2O_2 could be a scavenger for •OH (An 2023). Therefore, 10 mM H_2O_2 was selected as the optimum reaction parameters. The catalyst dosage influence on phenol removal efficiency was exhibited in Figs. S6c-d. When the Cu^0@CuZ dosage was greater than 0.1 g/L, 100% phenol removal efficiency was achieved. Notably, the k value increased from 0.096 to 0.387 min^{-1} with an increase in catalyst dosage from 0.05 to 0.2 g/L, which is owing to that the higher catalyst dosage produces the more H_2O_2 activation sites to generate more •OH, leading to the good phenol removal efficiency. Nevertheless, with further increasing of Cu^0@CuZ dosage from 0.2 to 0.4 g/L led the k value decreased. This is mainly attributed to that the superfluous catalysts could reduce the solution transmittance, resulting in light scattering, and the sum total of photons eventually reaching the surface of catalyst would be reduced.

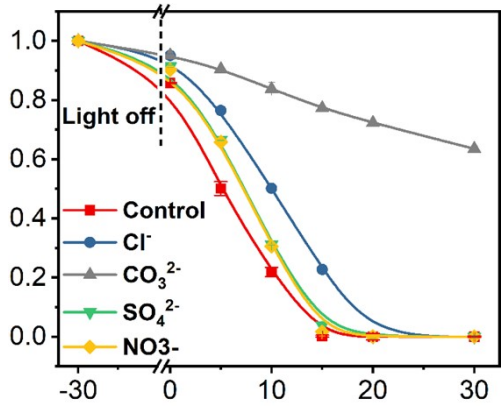

Fig. S9 Effects of coexisting anions on phenol removal efficiency over Cu^0@CuZ.

The addition of CO_3^{2-} inhibited the phenol removal efficiency by 63%. The reasons for the decrease are as follows: CO_3^{2-}, as trapping agent for •OH, would react with •OH to generate $•CO_3^-$ with weak oxidation ability; CO_3^{2-} in the water bodies can easily form HCO_3^-, OH^-, and H_2CO_3, leading to an increase in reaction system pH value (Eqs. 1−3), and the catalytic activity of the Cu^0@CuZ would be hindered.

$$CO_3^{2-} + •OH \rightarrow •CO_3^- + OH \quad (1)$$

$$CO_3^{2-} + H_2O \rightarrow HCO_3^- + OH^- \quad (2)$$

$$HCO_3^- + H_2O \rightarrow H_2CO_3 + OH^- \quad (3)$$

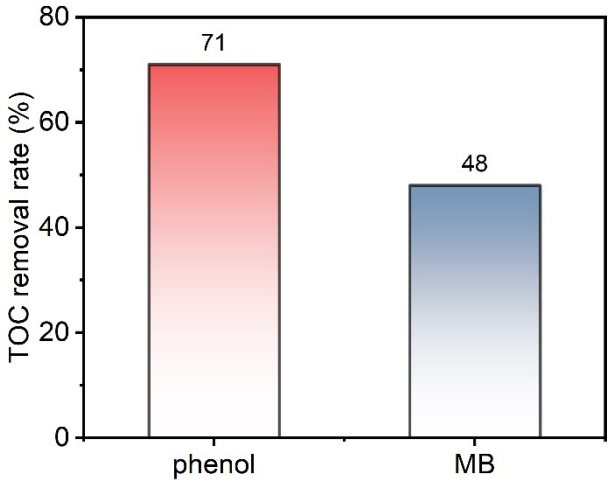

Fig. S10 The TOC removal rate of phenol and MB over Cu^0@CuZ in photo-Fenton-like system within 90 min.

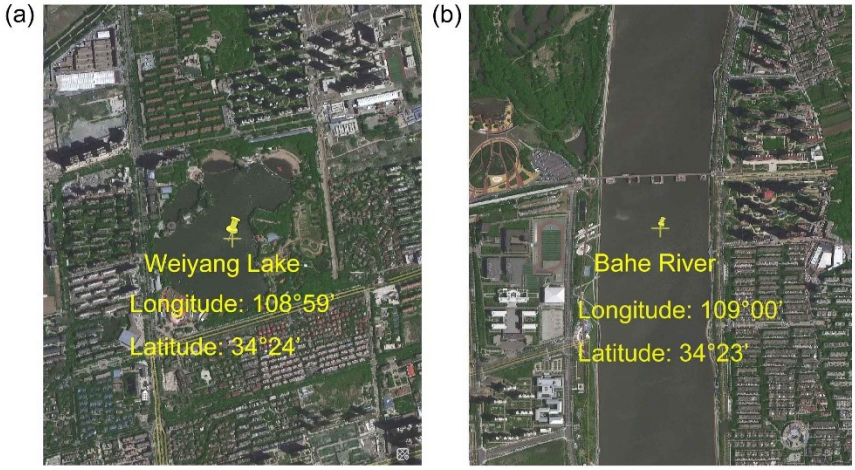

Fig. S11 (a) Lake water and (b) river water intake point.

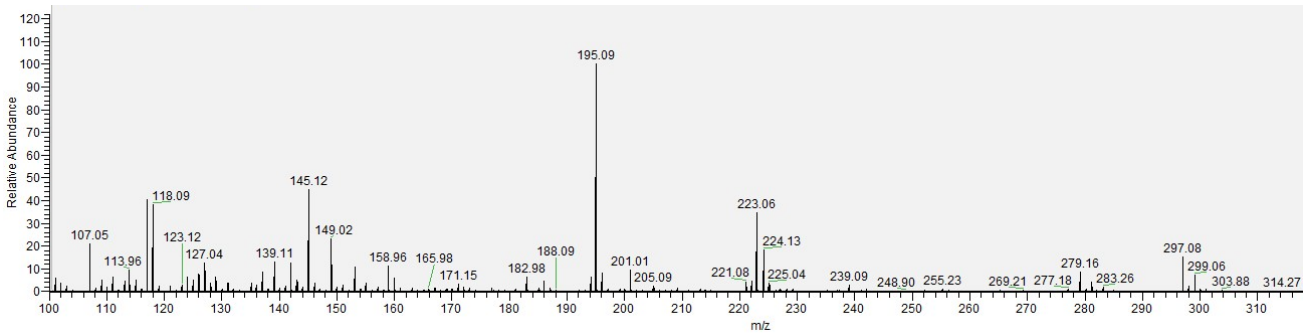

Fig. S12 Mass spectrum peak obtained from the DCF degradation over Cu^0@CuZ after 10 min irradiation.

References

1. M. Frisch, G. Trucks, H. Schlegel, G. Scuseria, M. Robb, J. Cheeseman, G. Scalmani, V. Barone, G. Petersson and H. Nakatsuji, Gaussian, Inc., Wallingford CT, 2016, *Gaussian09, Revision D*, 20 16, **1**.
2. T. Lu and F. Chen, Multiwfn: a multifunctional wavefunction analyzer, *J. Comput. Chem.*, 2012, **33**, 580-592.
3. T. Lu and Q. Chen, in *Conceptual Density Functional Theory*, 2022, DOI: 10.1002/978352782994 1.ch31, pp. 631-647.
4. R. G. Parr and W. T. Yang, Density Functional-Approach to the Frontier-Electron Theory of Che mical-Reactivity, *J. Am. Chem. Soc.*, 1984, **106**, 4049-4050.
5. J. Hu, J. Li, J. Cui, W. An, L. Liu, Y. Liang and W. Cui, Surface oxygen vacancies enriched F eOOH/Bi_2MoO_6 photocatalysis-Fenton synergy degradation of organic pollutants, *J. Hazard. Mater.*, 2020, **384**, 121399.
6. L. Yu, J. Chen, Z. Liang, W. Xu, L. Chen and D. Ye, Degradation of phenol using Fe_3O_4-GO n anocomposite as a heterogeneous photo-Fenton catalyst, *Sep. Purif. Technol.*, 2016, **171**, 80–87.
7. X. Qian, Y. Wu, M. Kan, M. Fang, D. Yue, J. Zeng and Y. Zhao, FeOOH quantum dots couple d g-C_3N_4 for visible light driving photo-Fenton degradation of organic pollutants, *Appl. Catal. B*, 2018, **237**, 513–520.
8. A. Fiorentino, R. Cucciniello, A. Di Cesare, D. Fontaneto, P. Prete, L. Rizzo, G. Corno and A. Proto, Disinfection of urban wastewater by a new photo-Fenton like process using Cu-iminodisucci nic acid complex as catalyst at neutral pH, *Water Res.*, 2018, **146**, 206-215.
9. P. K. Boruah, B. Sharma, I. Karbhal, M. V. Shelke and M. R. Das, Ammonia-modified graphene sheets decorated with magnetic Fe_3O_4 nanoparticles for the photocatalytic and photo-Fenton degrad ation of phenolic compounds under sunlight irradiation, *J. Hazard. Mater.*, 2017, **325**, 90-100.
10. P. Garcia-Muñoz, F. Fresno, C. Lefevre, D. Robert and N. Keller, Highly robust $La_{1-x}Ti_xFeO_3$ dua l catalyst with combined photocatalytic and photo-CWPO activity under visible light for 4-chlorop henol removal in water, *Appl. Catal. B*, 2020, **262**, 118310.
11. Z. Zhao, X. Cai, S. Fan, Y. Zhang, Z. Huang, H. Hu, J. Liang and Y. Qin, Construction of a st able Cu-Fe@C composite catalyst with enhanced performance and recyclability for visible-light-dri ven photo-Fenton reaction, *J. Alloys Compd.*, 2021, **877**, 160260.
12. Y. Li, X. Wang, Z. Duan, D. Yu, Q. Wang, D. Ji and W. Liu, Zn/Co-ZIFs@MIL-101(Fe) metal-organic frameworks are effective photo-Fenton catalysts for RhB removal, *Sep. Purif. Technol.*, 20 22, **293**, 121099.
13. M. Liu, H. Xia, W. Yang, X. Liu, J. Xiang, X. Wang, L. Hu and F. Lu, Novel Cu-Fe Bi-metal oxide quantum dots coupled g-C_3N_4 nanosheets with H_2O_2 adsorption-activation trade-off for effici ent photo-Fenton catalysis, *Appl. Catal. B*, 2022, **301**, 120765.
14. A. Corma, V. Fornes, S. B. Pergher, T. L. M. Maesen and J. G. Buglass, Delaminated zeolite pr ecursors as selective acidic catalysts, *Nature*, 1998, **396**, 353-356.

15. H.-K. Min, S. Kweon, S. Oh, H. An, Y. Cho, H. Min, D. Jo, J. F. Kim, C.-H. Shin, S. B. Kang and M. B. Park, Single-step preparation of zinco- and aluminosilicate delaminated MWW layers f or the catalytic conversion of glucose, *Green Chem.*, 2021, **23**, 9489-9501.
16. L. Singh, P. Rekha and S. Chand, Cu-impregnated zeolite Y as highly active and stable heterogen eous Fenton-like catalyst for degradation of Congo red dye, *Sep. Purif. Technol.*, 2016, **170**, 321-336.